

Inclusive K^+ and exclusive K^+Y photoproduction on the deuteron: Λ - and Σ -threshold phenomena

H. Yamamura, K. Miyagawa

*Department of Applied Physics, Okayama University of Science
1-1 Ridai-cho, Okayama 700, Japan*

T. Mart

Jurusan, Fisika, FMIPA, Universitas Indonesia, Depok 16424, Indonesia

C. Bennhold

*Center for Nuclear Studies, Department of Physics, The George Washington University,
Washington, D.C. 20052, USA*

W. Glöckle

Institut für Theoretische Physik II, Ruhr-Universität Bochum, D-44780 Bochum, Germany

Abstract

Inclusive K^+ and exclusive K^+Y photoproduction on the deuteron are investigated theoretically. Modern hyperon-nucleon forces and a recently updated kaon photoproduction operator for the $\gamma + N \rightarrow K^+ + Y$ process are used. Sizable effects of the hyperon-nucleon final state interaction are found near the $K^+\Lambda N$ and $K^+\Sigma N$ thresholds in the inclusive reaction. Angular distributions for the exclusive process show clear YN final state interaction effects in certain kinematic regions. Precise data especially for the inclusive process around the $K^+\Sigma N$ threshold would help to clarify the strength and property of the ΛN - ΣN interaction.

25.20.Lj, 13.75.Ev, 13.60.Le, 21.45.+v

I. INTRODUCTION

Despite many investigations in the realm of hypernuclear physics [1] many properties of the hyperon-nucleon interaction remain uncertain. In the case of the NN forces one has the rich set of NN scattering data at one's disposal to adjust NN force parameters. Such a set is basically absent in the YN system. If one had had to extract the NN force properties from spectra of nuclei only, our knowledge on the NN forces would have been remained rather uncertain and limited. Few-body systems which can be solved rigorously can therefore play a helpful role to acquire more detailed information on the YN forces including the important Λ - Σ conversion. A first example is the hypertriton, where recent rigorous solutions [2] of the coupled ΛNN - ΣNN Schrödinger equation allowed to exclude certain YN forces which do not bind the hypertriton, assuming that that 3-body YNN forces are absent.

Calculations coming up on ${}^4_{\Lambda}\text{He}$ and ${}^4_{\Lambda}\text{H}$ [3] will supplement these studies on ${}^3_{\Lambda}\text{H}$ and, because of their richer spectra [4], will be even more informative. For the purpose of investigating Λ - Σ conversion, scattering processes which cover a wide range of energies from the Λ to the Σ threshold and beyond appear to be especially informative.

In a recent study [5] the S -matrix pole structure for the YN system has been investigated for various presently used YN forces. As is well known there is no bound state in the $\Lambda(\Sigma)N$ system, but the present potential models support poles of the S -matrix which are close to the Λ and Σ thresholds. Near the Λ threshold there are two S -wave virtual states at about -3 and -5 MeV, and close to the Σ threshold there is a 3S_1 - 3D_1 pole which appears at different unphysical sheets of the Riemann energy surface depending on the potential used. This pole causes cusp-like structures in the ΛN scattering at the Σ threshold. Their forms and strengths depend on the potential employed.

Since performing hyperon-nucleon scattering experiments is very difficult, hyperon production processes on the deuteron, such as $\gamma(d, K^+)YN$, appear as natural candidates that allow exploring the the YN interaction. The hope is that the pole structure of the YN t -operator will have visible effects in such a production process. Pioneering work in inclusive and exclusive K^+ photoproduction on the deuteron has been done before [6] based on simple hyperon-nucleon forces. These calculations suggested that significant YN final-state interaction effects be present near the production thresholds. Inclusive electron induced K^+ production on the deuteron using modern YN forces appeared in [7]. In this article we reexamine the inclusive and exclusive photoproduction processes using various recently formulated YN forces [8,9] together with realistic NN forces and an updated elementary photoproduction operator [10] of the K^+Y pair on a nucleon. For the convenience of the reader the form of the production operator is presented in Sec. II. Section III describes the evaluation of the nuclear matrix element and the inclusive cross section, while Section IV is devoted to the exclusive cross section. Our numerical results for the various YN forces are displayed in Sec. V. We conclude in Sec. VI.

II. THE PRODUCTION OPERATOR

Almost all analyses of kaon photoproduction on the nucleon were performed at tree level [11] in an effective Lagrangian approach. While this leads to violation of unitarity, this kind of isobaric model provides a simple tool to parameterize kaon photoproduction off

the nucleon because it is relatively easy to calculate and to use for production on nuclei. Without rescattering contributions the T -matrix is simply approximated by the driving term alone which is assumed to be given by a series of tree-level diagrams. The selected Feynman diagrams for the s -, u -, and t -channel contain some unknown coupling parameters to be adjusted in order to reproduce experimental data. Final state interaction is effectively absorbed in these coupling constants which then cannot easily be compared to couplings from other reactions. Guided by recent coupled-channel results [12], Ref. [13] has reanalyzed the newest data [14] and constructed a tree-level amplitude that reproduces all available $K^+\Lambda$, $K^+\Sigma^0$ and $K^0\Sigma^+$ photoproduction data and thus provides an effective parameterization of these processes. The background terms included the standard s -, u -, and t -channel contributions along with a contact term that was required to restore gauge invariance after hadronic form factors had been introduced [15]. This model included the three nucleon resonances that have been found in the coupled-channels approach to decay into the $K\Lambda$ channel, the $S_{11}(1650)$, $P_{11}(1710)$, and $P_{13}(1720)$. For $K\Sigma$ production further contributions from the $S_{31}(1900)$ and $P_{31}(1910)$ Δ resonances were added.

Figure 1 shows total cross section calculations for the six different possible kaon photoproduction processes along with the newest data [14], comparing the model developed in Ref. [13] with an older version [10]. In order to obtain predictions for the reactions on the neutron, isospin symmetry was used for the strong vertices while the electromagnetic resonance couplings of the neutron were taken from the listing of helicity amplitudes in the Particle Data Tables. Below, we will only use the model of Ref. [13] for the calculations on the deuteron.

The relativistic operator has the form

$$\begin{aligned}
t_{\gamma K} = & \left(\frac{E_N + m_N}{2m_N} \right)^{\frac{1}{2}} \left(\frac{E_Y + m_Y}{2m_Y} \right)^{\frac{1}{2}} \sqrt{\frac{m_Y}{E_Y}} \sqrt{\frac{m_N}{E_N}} \times \\
& [\mathcal{F}_1 \boldsymbol{\sigma} \cdot \boldsymbol{\epsilon} + \mathcal{F}_4 \boldsymbol{\sigma} \cdot \mathbf{p}_\gamma \mathbf{p}_N \cdot \boldsymbol{\epsilon} + \mathcal{F}_5 \boldsymbol{\sigma} \cdot \mathbf{p}_\gamma \mathbf{p}_Y \cdot \boldsymbol{\epsilon} + \mathcal{F}_8 \boldsymbol{\sigma} \cdot \mathbf{p}_N \mathbf{p}_N \cdot \boldsymbol{\epsilon} + \mathcal{F}_9 \boldsymbol{\sigma} \cdot \mathbf{p}_N \mathbf{p}_Y \cdot \boldsymbol{\epsilon} \\
& + \mathcal{F}_{12} \boldsymbol{\sigma} \cdot \mathbf{p}_Y \mathbf{p}_N \cdot \boldsymbol{\epsilon} + \mathcal{F}_{13} \boldsymbol{\sigma} \cdot \mathbf{p}_Y \mathbf{p}_Y \cdot \boldsymbol{\epsilon} + \mathcal{F}_{14} \boldsymbol{\sigma} \cdot \boldsymbol{\epsilon} \boldsymbol{\sigma} \cdot \mathbf{p}_\gamma \boldsymbol{\sigma} \cdot \mathbf{p}_N + \mathcal{F}_{15} \boldsymbol{\sigma} \cdot \mathbf{p}_Y \boldsymbol{\sigma} \cdot \boldsymbol{\epsilon} \boldsymbol{\sigma} \cdot \mathbf{p}_\gamma \\
& + \mathcal{F}_{16} \boldsymbol{\sigma} \cdot \mathbf{p}_Y \boldsymbol{\sigma} \cdot \boldsymbol{\epsilon} \boldsymbol{\sigma} \cdot \mathbf{p}_N + \mathcal{F}_{19} \boldsymbol{\sigma} \cdot \mathbf{p}_Y \boldsymbol{\sigma} \cdot \mathbf{p}_\gamma \boldsymbol{\sigma} \cdot \mathbf{p}_N \mathbf{p}_N \cdot \boldsymbol{\epsilon} \\
& + \mathcal{F}_{20} \boldsymbol{\sigma} \cdot \mathbf{p}_Y \boldsymbol{\sigma} \cdot \mathbf{p}_\gamma \boldsymbol{\sigma} \cdot \mathbf{p}_N \mathbf{p}_Y \cdot \boldsymbol{\epsilon}] , \tag{2.1}
\end{aligned}$$

where m_N and m_Y denote the nucleon and hyperon masses, E_N and E_Y their energies, \mathbf{p}_γ , \mathbf{p}_N and \mathbf{p}_Y the photon, nucleon and hyperon momenta and $\boldsymbol{\epsilon}$ the photon polarization. These momenta together with the K^+ momentum \mathbf{p}_K are constrained by three-momentum conservation but otherwise the operator $t_{\gamma K}$ is off-the-energy-shell when used inside a nucleus. Since the elementary process is described using Feynman diagrams – rather than multipole amplitudes – the operator can be taken off-mass shell in a straightforward manner. The amplitudes \mathcal{F}_i are given in terms of kinematical quantities and amplitudes A_i which are related to the various tree diagrams. The rather lengthy expressions of \mathcal{F}_i and A_i can be found in Ref. [18]. Note that the expression in Eq. (2.1) is valid in any frame.

It can be obviously rewritten into another form, which is also very convenient for applications

$$t_{\gamma K} = i (L + i \boldsymbol{\sigma} \cdot \mathbf{K}) , \quad (2.2)$$

where

$$L = N \{ -(\mathcal{F}_{14} + \mathcal{F}_{15} - \mathcal{F}_{16}) \mathbf{p}_N \cdot (\mathbf{p}_\gamma \times \boldsymbol{\epsilon}) + \mathcal{F}_{15} \mathbf{p}_K \cdot (\mathbf{p}_\gamma \times \boldsymbol{\epsilon}) - \mathcal{F}_{16} \mathbf{p}_N \cdot (\mathbf{p}_K \times \boldsymbol{\epsilon}) \\ - [(\mathcal{F}_{19} + \mathcal{F}_{20}) \mathbf{p}_N \cdot \boldsymbol{\epsilon} - \mathcal{F}_{20} \mathbf{p}_K \cdot \boldsymbol{\epsilon}] \mathbf{p}_N \cdot (\mathbf{p}_K \times \mathbf{p}_\gamma) \} \quad (2.3)$$

and

$$\mathbf{K} = -N (T_1 \boldsymbol{\epsilon} + T_2 \mathbf{p}_\gamma + T_3 \mathbf{p}_N + T_4 \mathbf{p}_K) , \quad (2.4)$$

with

$$T_1 = \mathcal{F}_1 + (\mathcal{F}_{14} - \mathcal{F}_{15} - \mathcal{F}_{16}) \mathbf{p}_N \cdot \mathbf{p}_\gamma + \mathcal{F}_{15} (\mathbf{p}_K \cdot \mathbf{p}_\gamma - \mathbf{p}_\gamma^2) + \mathcal{F}_{16} (\mathbf{p}_N \cdot \mathbf{p}_K - \mathbf{p}_N^2) , \quad (2.5)$$

$$T_2 = [\mathcal{F}_4 + \mathcal{F}_5 + \mathcal{F}_{12} + \mathcal{F}_{13} - \mathcal{F}_{14} + \mathcal{F}_{15} + \mathcal{F}_{16} + (\mathbf{p}_N \cdot \mathbf{p}_K - \mathbf{p}_N^2)(\mathcal{F}_{19} + \mathcal{F}_{20})] \mathbf{p}_N \cdot \boldsymbol{\epsilon} \\ - [\mathcal{F}_5 + \mathcal{F}_{13} + \mathcal{F}_{15} + (\mathbf{p}_N \cdot \mathbf{p}_K - \mathbf{p}_N^2) \mathcal{F}_{20}] \mathbf{p}_K \cdot \boldsymbol{\epsilon} , \quad (2.6)$$

$$T_3 = [\mathcal{F}_8 + \mathcal{F}_9 + \mathcal{F}_{12} + \mathcal{F}_{13} + 2\mathcal{F}_{16} + (2\mathbf{p}_N \cdot \mathbf{p}_\gamma + \mathbf{p}_\gamma^2 - \mathbf{p}_K \cdot \mathbf{p}_\gamma)(\mathcal{F}_{19} + \mathcal{F}_{20})] \mathbf{p}_N \cdot \boldsymbol{\epsilon} \\ - [\mathcal{F}_9 + \mathcal{F}_{13} + \mathcal{F}_{16} + (2\mathbf{p}_N \cdot \mathbf{p}_\gamma + \mathbf{p}_\gamma^2 - \mathbf{p}_K \cdot \mathbf{p}_\gamma) \mathcal{F}_{20}] \mathbf{p}_K \cdot \boldsymbol{\epsilon} , \quad (2.7)$$

$$T_4 = -[\mathcal{F}_{12} + \mathcal{F}_{13} + \mathcal{F}_{16} + \mathbf{p}_N \cdot \mathbf{p}_\gamma (\mathcal{F}_{19} + \mathcal{F}_{20})] \mathbf{p}_N \cdot \boldsymbol{\epsilon} + (\mathcal{F}_{13} + \mathbf{p}_N \cdot \mathbf{p}_\gamma \mathcal{F}_{20}) \mathbf{p}_K \cdot \boldsymbol{\epsilon} . \quad (2.8)$$

Furthermore, we have

$$N = \left(\frac{E_N + m_N}{2m_N} \right)^{\frac{1}{2}} \left(\frac{E_Y + m_Y}{2m_Y} \right)^{\frac{1}{2}} \sqrt{\frac{m_Y}{E_Y}} \sqrt{\frac{m_N}{E_N}} . \quad (2.9)$$

III. THE INCLUSIVE CROSS SECTION

The cross section for the inclusive process $d(\gamma, K^+)$ is given as

$$\begin{aligned}
d\sigma = & \frac{1}{6} \sum_Y \sum_{\mu_d \epsilon} \sum_{\mu_Y \mu_N} \sum_{\nu_Y \nu_N} \frac{(2\pi)^3}{4E_K E_\gamma} \int \frac{d\mathbf{p}_K}{(2\pi)^3} \frac{d\mathbf{p}_Y}{(2\pi)^3} \frac{d\mathbf{p}_N}{(2\pi)^3} \\
& \times \left| \sqrt{2} \langle \Psi_{\mathbf{q}_Y \mu_Y \nu_Y \mu_N \nu_N}^{(-)} | t_{\gamma K}(1) | \Psi_d \mu_d \rangle \right|^2 \times (2\pi)^4 \delta^{(4)}(P_d + Q - p_Y - p_N) , \quad (3.1)
\end{aligned}$$

where the μ 's and ν 's are spin and isospin magnetic quantum numbers and ϵ denotes the two photon polarizations. The states Ψ refer to the two baryons only and \mathbf{q}_Y is the (non-relativistic) relative momentum of the final hyperon and nucleon. The sum over Y refers to the Λ and Σ channels. The dependencies on the K^+ and photon parameters, aside from the normalization factors shown explicitly, are absorbed into the $t_{\gamma K}$ operator. In Eq. (3.1) we have also introduced the momentum transfer $Q = p_\gamma - p_K$. The factor $\sqrt{2}$ comes from proper antisymmetrization and the argument 1 in $t_{\gamma K}(1)$ indicates that it acts only on particle 1, which in the final state is given by the hyperon. Equation (3.1) can be easily derived via Feynman rules but using (inconsistently) nonrelativistic two-baryon wavefunctions. This derivation has the nice feature that it shows how to use the single particle operator introduced in Sec. II between the wavefunctions. Note that the factors $\sqrt{\frac{m_Y}{E_Y}} \sqrt{\frac{m_N}{E_N}}$ in Eq. (2.1) should be kept as a part of the operator. We point out that we have used plane waves for the kaons. While the final-state interaction of the kaon with the hyperon is effectively absorbed in the elementary amplitude the interaction of between the kaon and the spectator nucleon is neglected. However, since the K^+N interaction is rather weak on a hadronic scale we expect the effect of this omission to be negligible. In the nuclear matrix element appearing in Eq. (3.1) the corresponding hyperon and nucleon momenta are integrated over.

The kinematics and the elementary operator is kept in its relativistic form. Though this is somewhat inconsistent in relation to the nonrelativistic wave functions we believe it is a step in the right direction. The estimates [6] for relativistic effects related to the deuteron wavefunction turned out to be insignificant.

We note that we shall work throughout in the zero total momentum frame of the final two baryons. The integrations in Eq. (3.1) can be easily carried out in the c.m. frame of the final two baryons. To do that we supplement the expression (3.1) with $\frac{m_Y m_N}{E_Y E_N} \times \frac{E_Y E_N}{m_Y m_N}$. The second factor multiplies the nuclear matrix element, which again is treated non-relativistically. Thus, the second factor is replaced by unity. We end up with the result

$$\begin{aligned}
\frac{d\sigma}{dp_K d\Omega_K} = & \frac{\mathbf{p}_K^2}{(2\pi)^2 4E_\gamma E_K W} \sum_Y m_Y m_N |\mathbf{q}_Y| \\
& \times \frac{1}{6} \sum_{\mu_d \epsilon} \sum_{\mu_Y \mu_N} \sum_{\nu_Y \nu_N} \int d\hat{\mathbf{q}}_Y \left| \sqrt{2} \langle \Psi_{\mathbf{q}_Y \mu_Y \nu_Y \mu_N \nu_N}^{(-)} | t_{\gamma K}(1) | \Psi_d \mu_d \rangle \right|^2 , \quad (3.2)
\end{aligned}$$

where $W^2 = (P_d + Q)^2$ and $|\mathbf{q}_Y|$ is determined by the energy conserving delta function. The nuclear matrix element can be conveniently rewritten by applying the Möller wave operator generating the final scattering state to the right. One obtains

$$\begin{aligned}
\langle \Psi_{\mathbf{q}_Y \mu_Y \nu_Y \mu_N \nu_N}^{(-)} | t_{\gamma K}(1) | \Phi_{d\mu_d} \rangle &= \langle \mathbf{q}_Y \mu_Y \nu_Y \mu_N \nu_N | (1 + tG_0)t_{\gamma K}(1) | \Psi_{d\mu_d} \rangle \\
&\equiv \langle \mathbf{q}_Y \mu_Y \nu_Y \mu_N \nu_N | T | \Psi_{d\mu_d} \rangle .
\end{aligned} \tag{3.3}$$

Since we allow for Λ - Σ conversion, the state $\langle \Psi_{\mathbf{q}_Y \mu_Y \nu_Y \mu_N \nu_N}^{(-)} |$ is a row with a Λ and a Σ component. Similarly the free state $\langle \mathbf{q}_Y \mu_Y \nu_Y \mu_N \nu_N |$ has two components ($\langle \mathbf{q}_\Lambda \mu_\Lambda \nu_\Lambda \mu_N \nu_N |$, 0) for $Y = \Lambda$ and (0, $\langle \mathbf{q}_\Sigma \mu_\Sigma \nu_\Sigma \mu_N \nu_N |$) for $Y = \Sigma$. The operators t and G_0 occurring in Eq. (3.3) are 2×2 matrices acting on Λ and Σ components. The operator $t_{\gamma K}(1)$ converts a nucleon into a hyperon and is therefore like the operator T a two-component object in Λ and Σ space.

Obviously, T applied to the deuteron state obeys the integral equation

$$T | \Psi_{d\mu_d} \rangle = t_{\gamma K}(1) | \Psi_{d\mu_d} \rangle + VG_0 T | \Psi_{d\mu_d} \rangle , \tag{3.4}$$

where V is the hyperon-nucleon force including Λ - Σ conversion and t in Eq. (3.3) is the corresponding t -operator as given by a Lippman-Schwinger equation. The energy entering the free two-baryon propagator G_0 which is a diagonal matrix is given non-relativistically as

$$e_Y = (P_d + Q)^2 - m_N - m_Y .$$

Let us now define

$$T | \Psi_{d\mu_d} \rangle = \begin{pmatrix} T_\Lambda | \Psi_{d\mu_d} \rangle \\ T_\Sigma | \Psi_{d\mu_d} \rangle \end{pmatrix} . \tag{3.5}$$

Then Eq. (3.4) takes the form of a coupled set:

$$T_Y | \Psi_{d\mu_d} \rangle = t_{\gamma K}^Y(1) | \Psi_{d\mu_d} \rangle + \sum_{Y'} V_{Y,Y'} G_0^{Y'} T_{Y'} | \Psi_{d\mu_d} \rangle . \tag{3.6}$$

Equation (3.6) contains the elementary operator $t_{\gamma K}^Y$ producing a specific hyperon Y . We solve this set, Eq. (3.6), in momentum space and partial wave decomposed. We introduce the basis $\langle q_Y \alpha | = \langle q_Y (ls) j m t m_t |$ with $l, s, j(m)$ being the relative orbital, total spin and total angular momentum (with magnetic quantum number) of the two baryon system and $t(m_t)$ the total two-baryon isospin (with magnetic quantum number). Then Eq. (3.6) turns into

$$\begin{aligned}
\langle q_Y \alpha | T_Y | \Psi_{d\mu_d} \rangle &= \langle q_Y \alpha | t_{\gamma K}^Y(1) | \Psi_{d\mu_d} \rangle \\
&+ \sum_{Y'} \sum_{\alpha'} \int_0^\infty dq'_{Y'} q'^2_{Y'} \langle q_Y \alpha | V_{Y,Y'} | q'_{Y'}, \alpha' \rangle
\end{aligned}$$

$$\times \frac{1}{e_Y - \frac{q_{Y'}^2}{2\mu_{Y'}} + i\epsilon} \langle q_{Y'}', \alpha' | T_{Y'} | \Psi_{d\mu_d} \rangle . \quad (3.7)$$

Note that the operator $t_{\gamma K}^Y(1)$ includes hyperon production on the proton and the neutron. Consequently, the resulting two baryons can be of different types. Applying the operator $t_{\gamma K}$ on $|\Psi_d\rangle$ with the isospin part of the deuteron written out explicitly yields

$$\begin{aligned} & t_{\gamma K}(1) |\Psi_{d\mu_d}\rangle \\ &= t_{\gamma k}(1) \frac{1}{\sqrt{2}} (|p(1)\rangle |n(2)\rangle - |n(1)\rangle |p(2)\rangle) |\Phi_{d\mu_d}\rangle \\ &= \frac{1}{\sqrt{2}} \left(|\Lambda(1)\rangle |n(2)\rangle \langle \Lambda | t_{\gamma k} | p \rangle + |\Sigma^0(1)\rangle |n(2)\rangle \langle \Sigma^0 | t_{\gamma k} | p \rangle \right. \\ &\quad \left. - |\Sigma^-(1)\rangle |p(2)\rangle \langle \Sigma^- | t_{\gamma k} | n \rangle \right) |\Phi_{d\mu_d}\rangle . \end{aligned} \quad (3.8)$$

The main task is the evaluation of the driving term in Eq. (3.7) based on the elementary operator $t_{\gamma K}$ from Sec. II. This single particle operator acts in the two-baryon space. We introduce the relative momentum between general hyperon and nucleon momenta \mathbf{k}_Y and \mathbf{k}_N as

$$\mathbf{q}_Y = \frac{m_N \mathbf{k}_Y - m_Y \mathbf{k}_N}{m_N + m_Y} , \quad (3.9)$$

and the relative momentum between general two nucleon momenta \mathbf{k}_1 and \mathbf{k}_2 as

$$\mathbf{q} = \frac{1}{2} (\mathbf{k}_1 - \mathbf{k}_2) . \quad (3.10)$$

Then we obtain in obvious notation

$$\begin{aligned} \langle q_Y \alpha | t_{\gamma K}^Y(1) | \Psi_{d\mu_d} \rangle &= \int d\hat{\mathbf{q}}_Y [Y_l^*(\hat{\mathbf{q}}_Y) \otimes \langle s |]_m^j \sum_{\tilde{Y}} C^{tY\tilde{Y}} t_{\gamma K}^{\tilde{Y}}(\mathbf{k}_Y, \mathbf{k}_1) \\ &\quad \times \sum_{l_d=0,2} [Y_{l_d}(\hat{\mathbf{q}}) \otimes |s_d\rangle]_{\mu_d}^{j_d} \phi_{l_d}(q) , \end{aligned} \quad (3.11)$$

where the sum over \tilde{Y} refers to the Λ , Σ^0 and Σ^- production processes and according to Eq. (3.8) the coefficient $C^{tY\tilde{Y}}$ is given as

$$C^{tY\tilde{Y}} = \begin{cases} \frac{1}{\sqrt{2}}C(0\frac{1}{2}t, 0 - \frac{1}{2}m_t) & \text{for } Y = \Lambda \text{ and } \tilde{Y} = \Lambda \\ \frac{1}{\sqrt{2}}C(1\frac{1}{2}t, 0 - \frac{1}{2}m_t) & \text{for } Y = \Sigma \text{ and } \tilde{Y} = \Sigma^0 \\ -\frac{1}{\sqrt{2}}C(1\frac{1}{2}t, -1\frac{1}{2}m_t) & \text{for } Y = \Sigma \text{ and } \tilde{Y} = \Sigma^- \end{cases}, \quad (3.12)$$

with $m_t = -\frac{1}{2}$.

For the sake of transparency we kept the notation for the momenta occurring on the right-hand side of Eq. (3.11) with their obvious meanings. But they should be expressed in terms of the relative momentum \mathbf{q}_Y and a given external momentum \mathbf{Q} as

$$\mathbf{k}_Y = \mathbf{q}_Y, \quad (3.13)$$

$$\mathbf{k}_1 = \mathbf{q}_Y - \mathbf{Q}, \quad (3.14)$$

$$\mathbf{q} = \mathbf{q}_Y - \frac{1}{2}\mathbf{Q}. \quad (3.15)$$

Now the form of Eq. (2.2) for $t_{\gamma K}$ is very convenient and we obtain

$$\begin{aligned} \langle q_Y \alpha | t_{\gamma K}^Y(1) | \Psi_d \mu_d \rangle &= \sum_{\tilde{Y}} C^{tY\tilde{Y}} \sum_{l_d} \sum_{m'm''} C(ls_j, m' m - m' m) C(l_d s_d j_d, m'' \mu_d - m'' \mu_d) \\ &\times \{ \delta_{s s_d} \delta_{m-m', \mu_d-m''} \int d\hat{\mathbf{q}}_Y Y_{lm'}^*(\hat{\mathbf{q}}_Y) iL^{\tilde{Y}} Y_{l_d m''}(\hat{\mathbf{q}}) \phi_{l_d}(q) \\ &- \sum_{\nu} C(1s_d s, \nu, \mu_d - m'', m - m') \frac{(-)^{s-s_d+1}}{\sqrt{\hat{s}}} \langle s || \sigma(1) || s_d \rangle \\ &\times \int d\hat{\mathbf{q}}_Y Y_{lm'}^*(\hat{\mathbf{q}}_Y) (-)^{\nu} K_{-\nu}^{\tilde{Y}} Y_{l_d m''}(\hat{\mathbf{q}}) \phi_{l_d}(q) \}, \end{aligned} \quad (3.16)$$

where the index \tilde{Y} for the operators L and $K_{-\nu}$ specifies the three individual production processes as already mentioned. We have chosen the reduced spin matrix element to have the form

$$\langle s || \sigma(1) || s_d \rangle = \sqrt{\hat{s} \cdot 6 \cdot \hat{s}_d} (-)^{-s_d} \left\{ \begin{matrix} s & s_d & 1 \\ \frac{1}{2} & \frac{1}{2} & \frac{1}{2} \end{matrix} \right\}. \quad (3.17)$$

The remaining two-fold integrals will be performed numerically.

Once the coupled set, Eq. (3.7), has been solved we obtain the hadronic matrix element from Eq. (3.3) as

$$\begin{aligned}
& \langle \Psi_{\mathbf{q}_Y \mu_Y \nu_Y \mu_N \nu_N}^{(-)} | t_{\gamma K}(1) | \Psi_d \mu_d \rangle \\
&= \sum_{lsjmt} \langle \mathbf{q}_Y \mu_Y \nu_Y \mu_N \nu_N | (ls)jmtm_t \rangle \langle (ls)jmtm_t | T | \Psi_d \mu_d \rangle \\
&= \sum_{lsjmt} C(ls, j, m - \mu_Y - \mu_N, \mu_Y + \mu_N) C(\frac{1}{2}, \frac{1}{2}, s, \mu_Y \mu_N) \\
&\quad \times Y_{lm - \mu_Y - \mu_N}(\hat{\mathbf{q}}_Y) C(t_Y \frac{1}{2} t, \nu_Y \nu_N m_t) \langle q_Y (ls)jmtm_t | T_Y | \Psi_d \mu_d \rangle . \tag{3.18}
\end{aligned}$$

The isospins t_Y of the hyperon are 0 and 1 for Λ and Σ , respectively. This leads to the final expression for the inclusive cross section from Eq. (3.2)

$$\begin{aligned}
\frac{d\sigma}{dp_K d\Omega_K} &= \frac{\mathbf{p}_K^2}{(2\pi)^2 4E_\gamma E_K W} \sum_Y m_Y m_N |\mathbf{q}_Y| \\
&\quad \times \frac{1}{6} \sum_{\mu_d \in lsjm} \sum_t \left| \sqrt{2} \langle q_Y (ls)jmtm_t | T_Y | \Psi_d \mu_d \rangle \right|^2 . \tag{3.19}
\end{aligned}$$

It turns out that the convergence in j is rather slow due to the plane wave part of the amplitude. Therefore, we treated that part separately without partial wave decomposition. Let j_{\max} be the total two-baryon angular momentum beyond which the final state interaction can be neglected. Then

$$\begin{aligned}
& \sum_{l,s,j > j_{\max}, m} \left| \sqrt{2} \langle q_Y (ls)jmtm_t | T_Y | \Psi_d \mu_d \rangle \right|^2 \\
&= \sum_{l,s,j > j_{\max}, m} \left| \sqrt{2} \langle q_Y (ls)jmtm_t | t_{\gamma k}^Y(1) | \Psi_d \mu_d \rangle \right|^2 \\
&= \sum_{\mu_Y \mu_N} \int d\hat{\mathbf{q}}_Y \left| \sqrt{2} \langle \mathbf{q}_Y \mu_Y \mu_N t m_t | t_{\gamma k}(1) | \Psi_d \mu_d \rangle \right|^2 \\
&\quad - \sum_{l,s,j \leq j_{\max}, m} \left| \sqrt{2} \langle q_Y (ls)jmtm_t | t_{\gamma k}^Y(1) | \Psi_d \mu_d \rangle \right|^2 . \tag{3.20}
\end{aligned}$$

The second part is then added to the corresponding sum ($j \leq j_{\max}$) with $t_{\gamma k}^Y(1)$ replaced by T_Y . In this manner the explicitly partial wave projected part is due only to FSI.

IV. THE EXCLUSIVE CROSS SECTION

The exclusive cross section for the process $\gamma(d, K^+Y)N$ follows easily from Eq. (3.2) as

$$\frac{d^5\sigma}{dp_k d\Omega_k d\Omega_Y} = \frac{\mathbf{p}_K^2}{(2\pi)^2 4E_\gamma E_K} \frac{m_Y m_N |\mathbf{q}_Y|}{W} \times \frac{1}{6} \sum_{\mu_d \in \mu_Y \mu_N} \sum_{\nu_Y \nu_N} \left| \sqrt{2} \langle \Psi_{\mathbf{q}_Y \mu_Y \nu_Y \mu_N \nu_N}^{(-)} | t_{\gamma K}(1) | \Psi_d \mu_d \rangle \right|^2 . \quad (4.1)$$

The events have to lie on a kinematical locus, which relates the K^+ and Y energies. This relation is given by

$$\left(\sqrt{\mathbf{q}_Y^2 + m_Y^2} + \sqrt{\mathbf{q}_Y^2 + m_N^2} \right)^2 = (P_d + Q)^2 . \quad (4.2)$$

Again we use a separation of the total amplitude into the plane wave part which is treated without partial wave decomposition and the part due to FSI which is partial wave decomposed. We write

$$\begin{aligned} & \sqrt{2} \langle \mathbf{q}_Y \mu_Y \nu_Y \mu_N \nu_N | T | \Psi_d \mu_d \rangle \\ &= \sum_s \sqrt{2} C\left(\frac{1}{2} s, \mu_Y \mu_N m_s\right) \langle s m_s | \mathbf{q}_Y \nu_Y \nu_N | t_{\gamma k}(1) | \Psi_d \mu_d \rangle \\ &+ \sum_{l,s,j,m} C\left(\frac{1}{2} s, \mu_Y \mu_N\right) (l s j, m - \mu_Y - \mu_N, \mu_Y + \mu_N) Y_{l m - \mu_Y - \mu_N}(\hat{\mathbf{q}}_Y) \\ &\quad \times \sqrt{2} \langle q_Y(l s) j m \nu_Y \nu_N | T_Y - t_{\gamma k}^Y(1) | \Psi_d \mu_d \rangle . \end{aligned} \quad (4.3)$$

V. RESULTS

In this study we compare results for the hyperon-nucleon forces NSC89 [8] and NSC97f [9]. Both lead to the correct hypertriton binding energy [2]. One of us (K.M.) recently investigated various new versions of the YN forces developed by the Nijmegen group [9]. Only the NSC97f force binds the hypertriton correctly. The deuteron wavefunction is generated by the Nijmegen93 potential [17]. The value j_{\max} up to which FSI had to be taken into account turned out to be $j_{\max} = 2$. The results presented below are given at a photon energy $E_\gamma = 1.3$ GeV. In Fig. 2, we compare the inclusive cross sections for $d(\gamma, K^+)$ in plane wave impulse approximation (PWIA) with calculations that include FSI. In order to obtain the largest cross section we have chosen $\theta_K = 0^\circ$. The two pronounced peaks around $p_K = 945$ and 809 MeV/c can be understood in PWIA. They are due to quasi-free processes, where one of the nucleons in the deuteron is a spectator and has zero momentum in the lab system. This then leads to a vanishing argument $q = 0$ in the deuteron wavefunction, which causes the peaks. Under this condition the kinematics of the γ -induced process on a single nucleon fixes the peak positions for p_K in the lab system.

We see deviations between the plane wave result and the results with FSI based on the NSC89 and NSC97f hyperon-nucleon forces. Near the $K^+\Lambda N$ threshold FSI enhance the cross section by up to 86%. Near the $K^+\Sigma N$ threshold the effects are also of interest. While NSC89 has hardly any effect, NSC97f leads to a prominent cusp-like structure. The neighborhood of the $K^+\Sigma N$ threshold is shown again enlarged in Fig. 3. The two YN potentials lead to predictions which differ by up to 35%. Different predictions of the two potentials are also seen in the total elastic ΛN cross section as depicted in Fig. 4. The peak for NSC97f is significantly higher near the ΣN threshold than for NSC89. As worked out in Ref. [5], this can be traced back to the location of the S -matrix pole for the ΛN - ΣN system around the ΣN threshold. We show in Fig. 5 the complex plane of the relative ΣN momentum $p_{\Sigma N}$. Each of the two YN potentials generates a pole in the state ${}^3S_1 - {}^3D_1$ near $p_{\Sigma N} = 0$. The potential NSC89 leads to a pole position which in a single channel case would be called a virtual state (in this case it would lie exactly on the imaginary axis). The coupling of the Λ and Σ channels moves the pole for the NSC97f force away from the positive imaginary axis into the second $p_{\Sigma N}$ quadrant. In a time-dependent description the energy related to that pole position leads to a decreasing amplitude. In the literature, this sort of pole is sometimes referred to as an ‘unstable bound state’. Apparently, the actual pole position depends on the details of the YN force. The pole positions are an inherent property of the YN forces and the actual location chosen by nature should be determined with the help of experimental measurements.

Another interesting insight into the inclusive cross section is shown in Fig. 6 for the PWIA calculation. The inclusive cross section is formed additively by the contributions for Λn , $\Sigma^0 n$ and $\Sigma^- p$ production. Above the $K^+\Sigma N$ threshold the Λn contribution becomes smaller while the two parts for $\Sigma^0 n$ and $\Sigma^- p$ production contribute about equally. Note that the $\Sigma^- p$ contribution results from the elementary K^+ production on the neutron.

There are many options to display the information contained in the exclusive cross section; we show in Figs. 7–10 angular distributions of the hyperons in the hyperon-nucleon c.m. frame for the K^+ meson emerging in the direction of the photon ($\theta_K = 0^\circ$). For $K^+\Lambda$ production we have chosen two K -meson momenta, $p_K = 972$ MeV/c, shown in Fig. 7, and $p_K = 870$ MeV/c, the region just below the $K^+\Sigma N$ threshold (Fig. 8). In both cases FSI effects are found to be significant. As shown in Fig. 7, the calculations including FSI lie considerably above the PWIA results. The difference between the two FSI results is small at this kinematics. Fig. 8 displays cross sections at $p_K = 870$ MeV/c, here the effect of FSI is to scatter Λ 's to larger angles compared to PWIA. At very backward angles the PWIA result is basically zero while the FSI calculations still show some strength.

In the case of $\Sigma^- p$ production we also present results at two different kaon momenta, one just above the Σ threshold and one in the peak region of the inclusive cross section. Fig. 9 shows dramatic differences not only between the PWIA and the FSI results but also between the calculations that employ the NSC97f and the NSC89 forces. For backward angles, the results differ by more than 50%. Measurements should easily be able to distinguish between these possibilities. In contrast, no differences are seen in Fig. 10, illustrating how important it is to choose the proper kinematics.

Further observables for the exclusive process, like energy distributions for fixed K^+ meson and hyperon angles, will be studied in a forthcoming article. Especially configurations where the relative energy between the hyperon and nucleon goes to zero might be of interest, since

this might allow extracting hyperon-nucleon scattering lengths. The poles in the hyperon-nucleon t -matrix near the thresholds will lead to enhancements, though not as spectacular as in the NN case [19]. Other quantities that will be studied include polarization observables which are especially accessible due to the self-analyzing property of the lambda. Thus, the lambda recoil polarization in combination with either linearly or circularly polarized photons could be measured at Jefferson Lab. The first measurements of kaon photoproduction on the deuteron are scheduled to take place later this year [20].

VI. CONCLUSION

We have evaluated the $\gamma(d, K^+)$ inclusive and the $\gamma(d, K^+Y)$ exclusive processes using the modern YN interactions NSC89 and NSC97f. Both include Λ - Σ conversion and give the correct ${}^3\Lambda\text{H}$ binding energy. The deuteron wavefunction was based on the Nijmegen93 NN potential. The aim was to search for final state interaction effects in the ΛN and ΣN systems. In the inclusive cross section we found effects near the $K^+\Lambda N$ and the $K^+\Sigma N$ thresholds which might be measurable. Especially for the latter case the two YN potential predictions are quite different, reflecting the different underlying S -matrix pole structure for the two YN forces. The exclusive process shows significant FSI effects which we displayed for the angular distributions of the hyperons. Around the $K^+\Sigma N$ threshold FSI effects are especially interesting and the two YN forces show quite different effects. Future data should easily be able to distinguish between the different YN forces.

ACKNOWLEDGMENTS

W.G. would like to thank the Deutsche Forschungsgemeinschaft for financial support and the Okayama University of Science for the warm hospitality. K.M. thanks the few-body group of the Ruhr University Bochum for the kind hospitality during his stay. C.B. acknowledges the support from DOE grant DE-FG02-95ER-40907. T.M. thanks the Okayama University of Science for the hospitality and acknowledges the University Research for Graduate Education (URGE) grant.

REFERENCES

- [1] *Proceedings of the International Conference on Hypernuclear and Strange Particle Physics*, edited by D. J. Millener and R. E. Chrien, Nucl. Phys. **A639** (1998).
- [2] K. Miyagawa, H. Kamada, W. Glöckle, and V. Stoks, Phys. Rev. C **51**, 2905 (1995); W. Glöckle, K. Miyagawa, H. Kamada, J. Golak, and H. Witala, Nucl. Phys. **A639**, 297c (1998).
- [3] E. Hiyama, M. Kamimura, T. Motoba, T. Yamada, and Y. Yamamoto, Nucl. Phys. **A639**, 169c (1998); E. Hiyama, private communication.
- [4] See B. F. Gibson and E. V. Hungerford, Phys. Rep. **257**, 349 (1995), and the references therein.
- [5] K. Miyagawa and H. Yamamura, Phys. Rev. C **60**, 024003 (1999); nucl-th/9904002.
- [6] R. A. Adelseck and L. E. Wright, Phys. Rev. C **39**, 580 (1989); X. Li and L. E. Wright, J. Phys. G: Nucl. Part. Phys. **17**, 1127 (1991); S. R. Cotanch and S. Hsiao, Nucl. Phys. **A450**, 419c (1986).
- [7] T.-S. H. Lee, V. Stoks, B. Saghai, and C. Fayard, Nucl. Phys. **A639**, 247c (1998).
- [8] P. M. M. Maessen, Th. A. Rijken, and J. J. de Swart, Phys. Rev. C **40**, 2226 (1989).
- [9] Th. A. Rijken, V. G. J. Stoks, and Y. Yamamoto, Phys. Rev. C **59**, 21 (1999).
- [10] C. Bennhold, T. Mart, and D. Kusno, in *Proceedings of the CEBAF/INT Workshop on N* Physics, Seattle, USA, 1996*, edited by T.-S. H. Lee and W. Roberts, (World Scientific, Singapore, 1997), p. 166.
- [11] J. C. David, C. Fayard, G. H. Lamot, and B. Saghai, Phys. Rev. C **53**, 2613 (1996); R. A. Williams, C.-R. Ji, and S. R. Cotanch, Phys. Rev. C **46**, 1617 (1992); T. Mart, C. Bennhold, and C. Hyde-Wright, Phys. Rev. C **51**, R1074 (1995); R. A. Adelseck, C. Bennhold, and L. E. Wright, Phys. Rev. C **32**, 1681 (1985).
- [12] T. Feuster and U. Mosel, Phys. Rev. C **58**, 457 (1998); Phys. Rev. C **59**, 460 (1999).
- [13] C. Bennhold, T. Mart, A. Waluyo, H. Haberzettl, G. Penner, T. Feuster, and U. Mosel, in *Proceedings of the Workshop on Electron-Nucleus Scattering, Elba, Italy, 1998*, edited by O. Benhar, A. Fabrocini, and R. Schiavilla (Edizioni ETS, Pisa, 1999), p. 149; nucl-th/9901066.
- [14] SAPHIR Collaboration, M.Q. Tran *et al.*, Phys. Lett. B **445**, 20 (1998).
- [15] H. Haberzettl, Phys. Rev. C **56**, 2041 (1997); H. Haberzettl, C. Bennhold, T. Mart, and T. Feuster, Phys. Rev. C **58**, R40 (1998).
- [16] Aachen-Berlin-Bonn-Hamburg-Heidelberg-München Collaboration, Phys. Rev. **188**, 2060 (1969). A list of references for the old data can be found in Ref. [14].
- [17] V. G. J. Stoks, R. A. M. Klomp, C. P. F. Terheggen, and J. J. de Swart, Phys. Rev. C **49**, 2950 (1994).
- [18] T. Mart, Ph.D Thesis, Universität Mainz, 1996 (unpublished); T. Mart, L. Tiator, D. Drechsel, and C. Bennhold, Nucl. Phys. **A640**, 235 (1998).
- [19] W. Glöckle, H. Witala, D. Hüber, H. Kamada, and J. Golak, Phys. Rep. **274**, 107 (1996).
- [20] B. Mecking *et al.*, CEBAF proposal PR-89-045 (1989).

FIGURES

FIG. 1. The six possible kaon photoproduction channels compared to new experimental data. The solid curve shows the model of Ref. [13] while the dashed line shows an older calculation of Ref. [10]. The new SAPHIR data [14] are denoted by the solid squares, old data [16] are shown by the open circles.

FIG. 2. The inclusive $\gamma(d, K^+)$ cross section as a function of lab momenta p_K for $\theta_K = 0^\circ$ and photon lab energy $E_\gamma = 1.3$ GeV. The plane wave result is compared to two YN force predictions. The FSI effects are especially pronounced near the $K^+\Lambda N$ and $K^+\Sigma N$ thresholds the locations of which are indicated by the arrows.

FIG. 3. The results of Fig. 2 enlarged around the $K^+\Sigma N$ threshold.

FIG. 4. The total ΛN elastic cross section as a function of the Λ lab momentum around the ΣN threshold indicated by the arrow. The NSC97f prediction leads to a more pronounced peak structure than the NSC89 prediction.

FIG. 5. The S -matrix pole positions for the ΛN - ΣN system in the complex $p_{\Sigma N}$ plane for the two modern YN forces NSC97f and NSC89 (see text).

FIG. 6. The inclusive $\gamma(d, K^+)$ cross section as a function of lab momenta p_K for $\theta_K = 0^\circ$ and photon lab energy $E_\gamma = 1.3$ GeV in plane wave approximation. The $K^+\Lambda N$ and $K^+\Sigma N$ thresholds are indicated by the arrows. The additive contributions for the Λn , $\Sigma^0 n$ and $\Sigma^- p$ processes are shown separately and summed up.

FIG. 7. The exclusive cross section $\gamma(d, K^+\Lambda)n$ cross section for $\theta_K = 0^\circ$, lab momentum $p_K = 972$ MeV/ c and photon lab energy $E_\gamma = 1.3$ GeV as a function of the Λ scattering angle in the ΛN c.m. system. The plane wave prediction is compared to two YN force calculations.

FIG. 8. The same as in Fig. 7 for $p_K = 870$ MeV/ c . The FSI effects scatter the Λ 's to larger angles than in PWIA.

FIG. 9. The exclusive cross section $\gamma(d, K^+\Sigma^-)p$ cross section for $\theta_K = 0^\circ$, lab momentum $p_K = 865$ MeV/ c and photon lab energy $E_\gamma = 1.3$ GeV as a function of the Σ^- scattering angle in the $\Sigma^- p$ c.m. system. The plane wave prediction is compared to two YN force calculations which are strikingly different.

FIG. 10. The same as in Fig. 9 for $p_K = 810$ MeV/ c .

Fig. 1

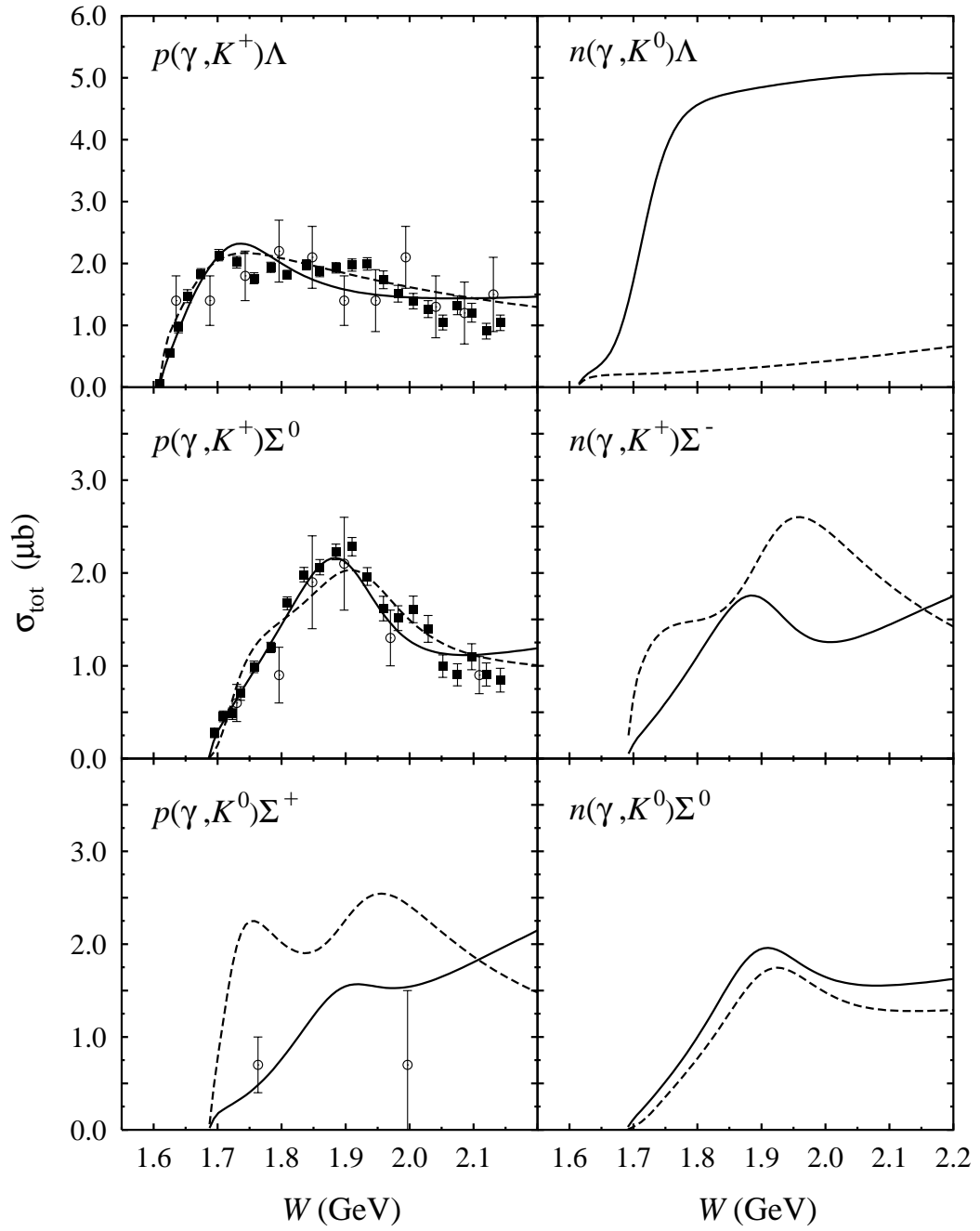


Fig. 2

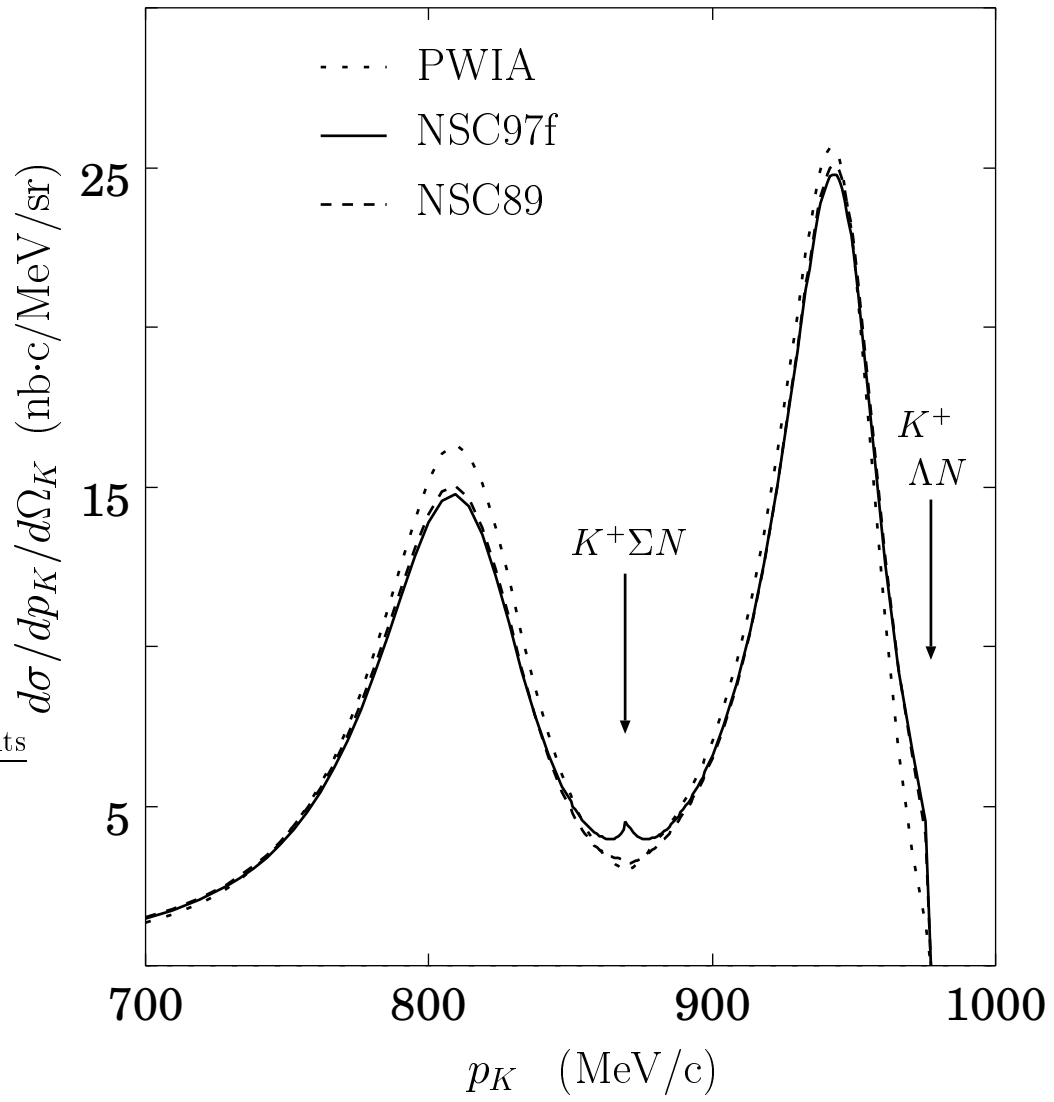


Fig. 3

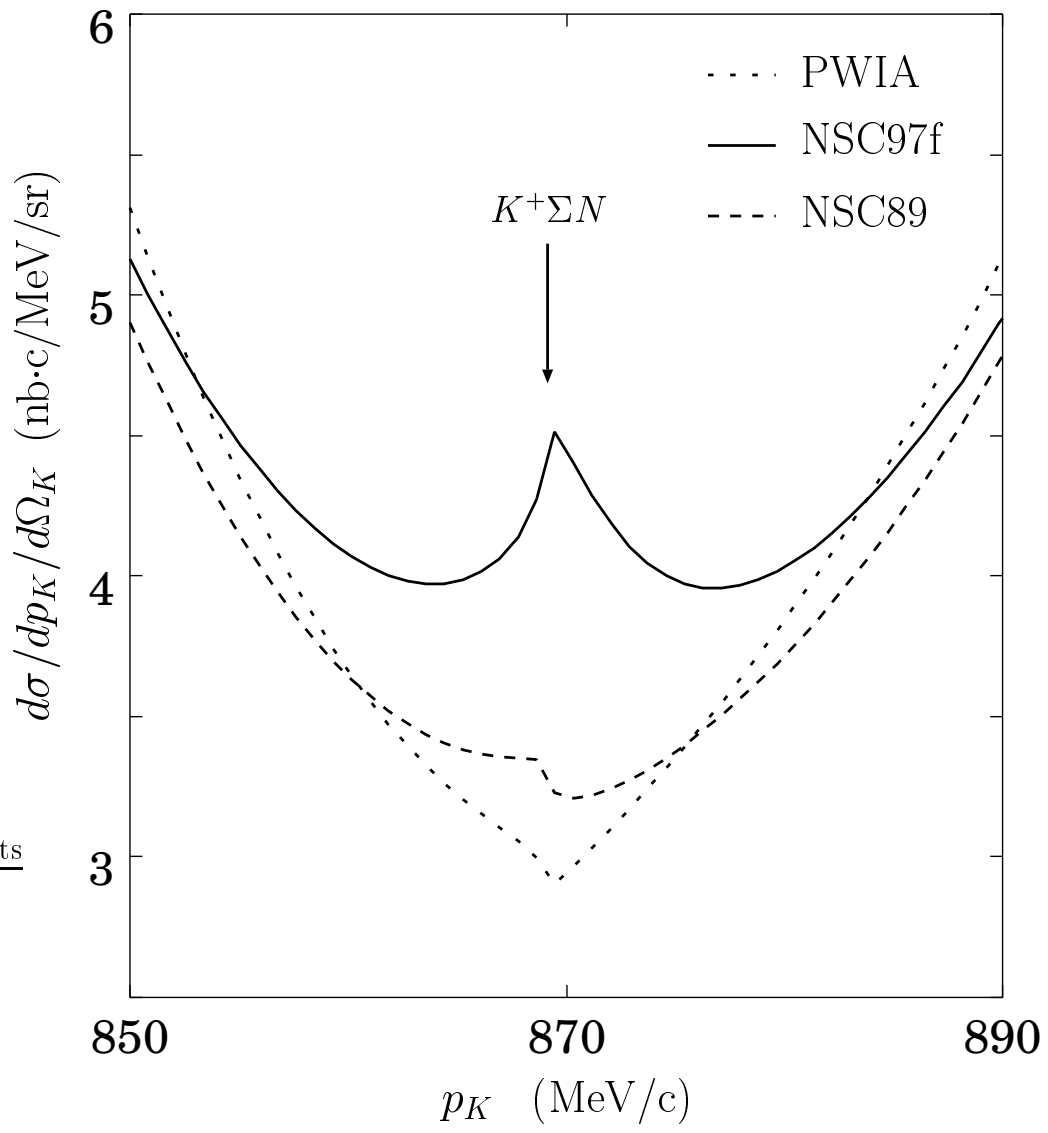


Fig. 4

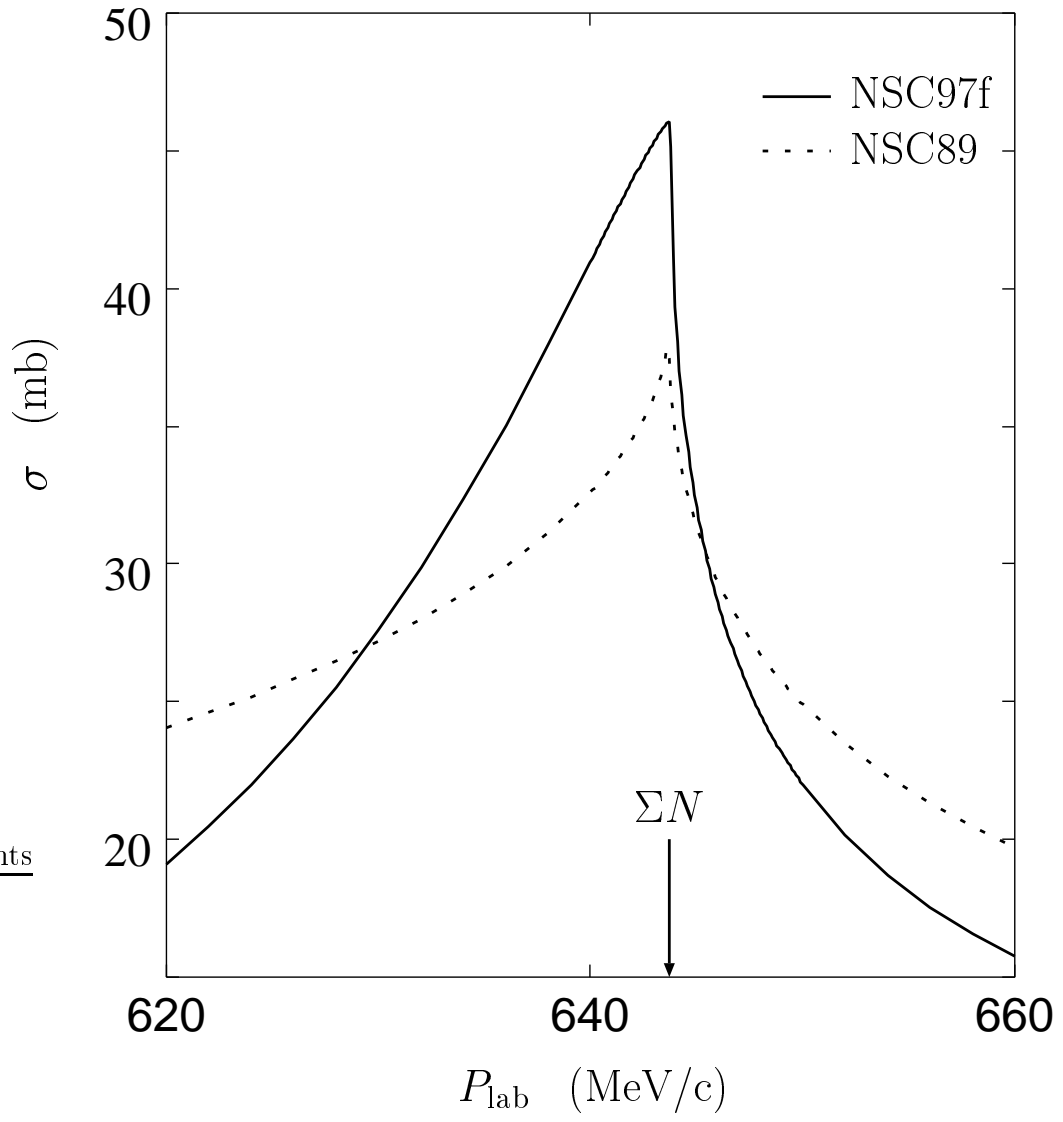


Fig. 5

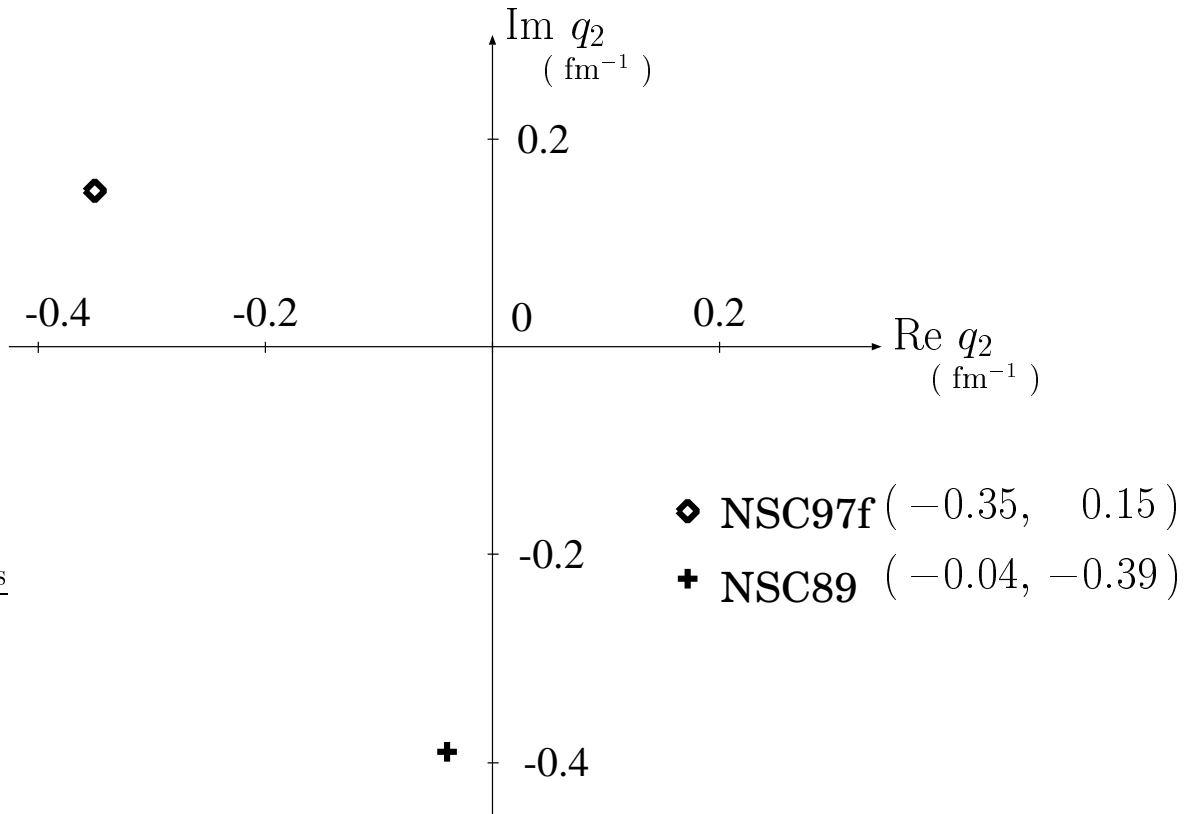


Fig. 6

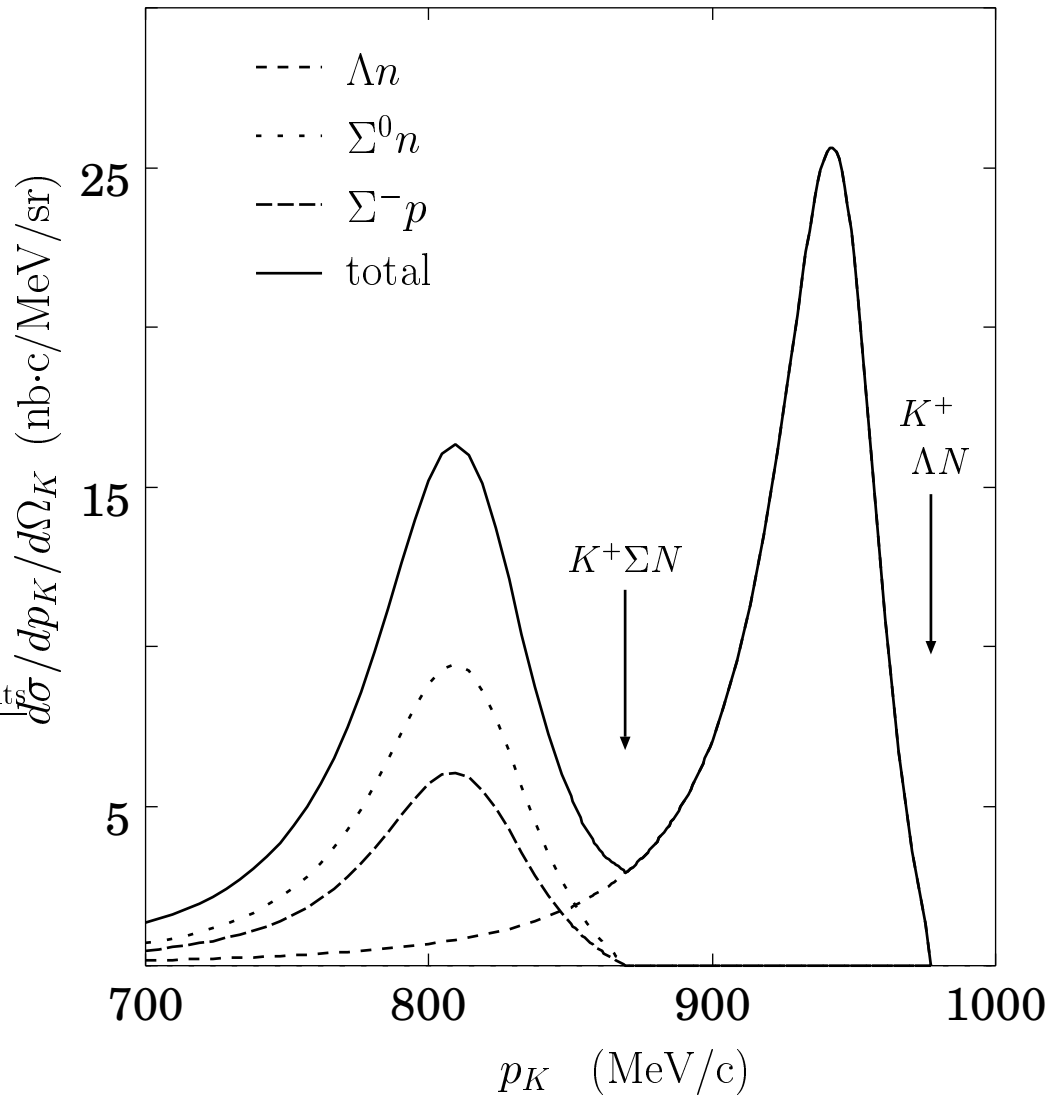


Fig. 7

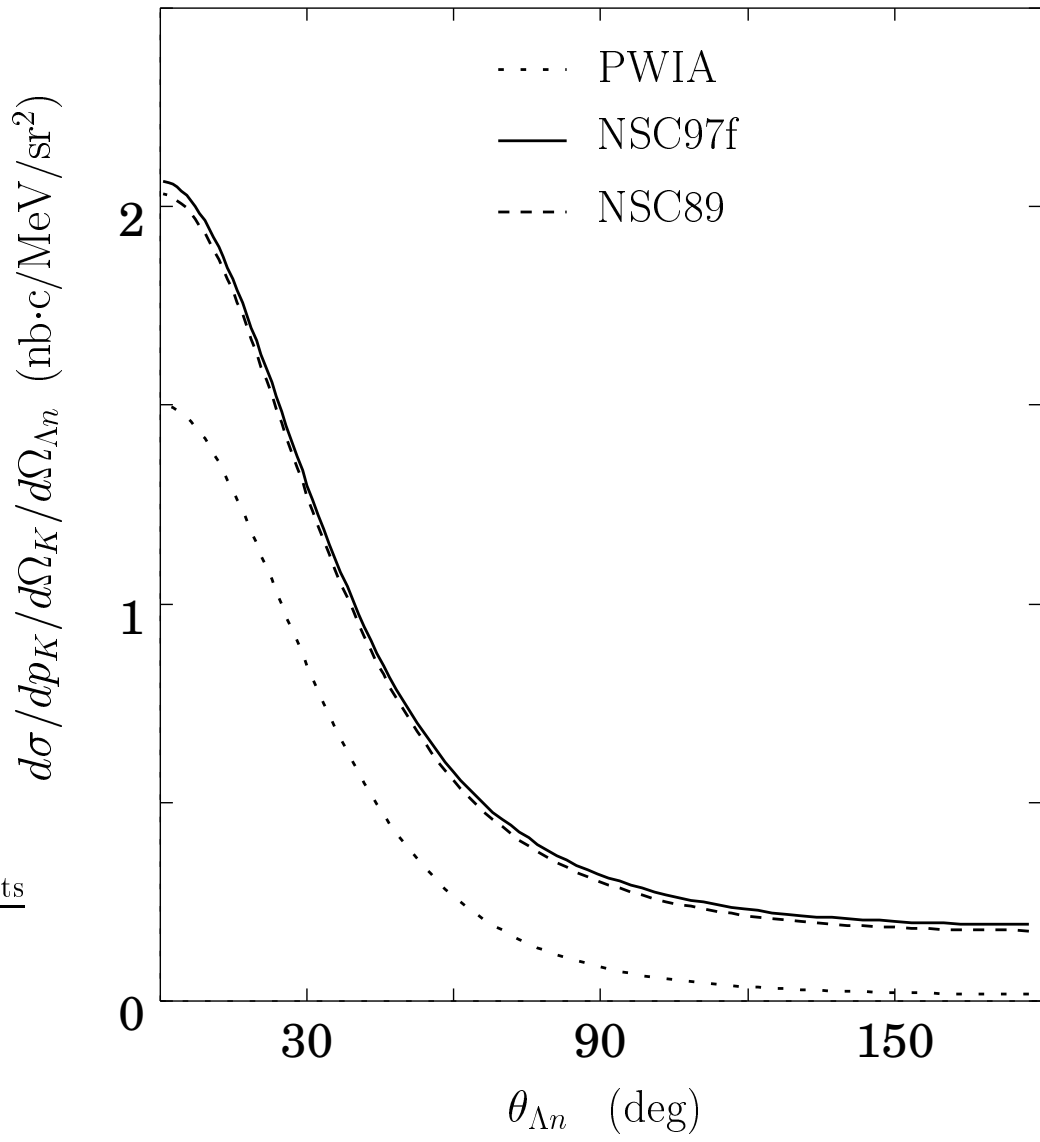


Fig. 8

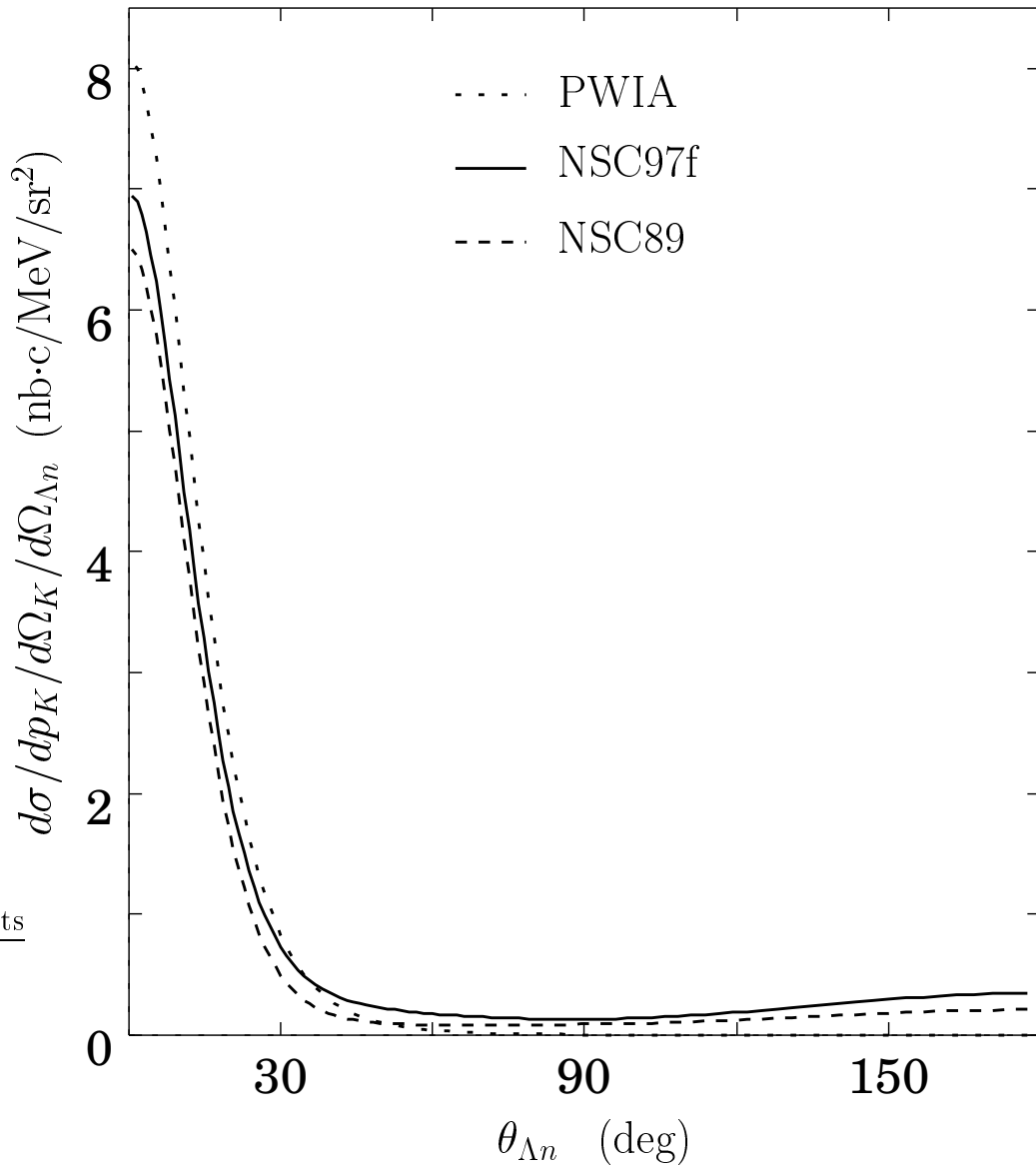


Fig. 9

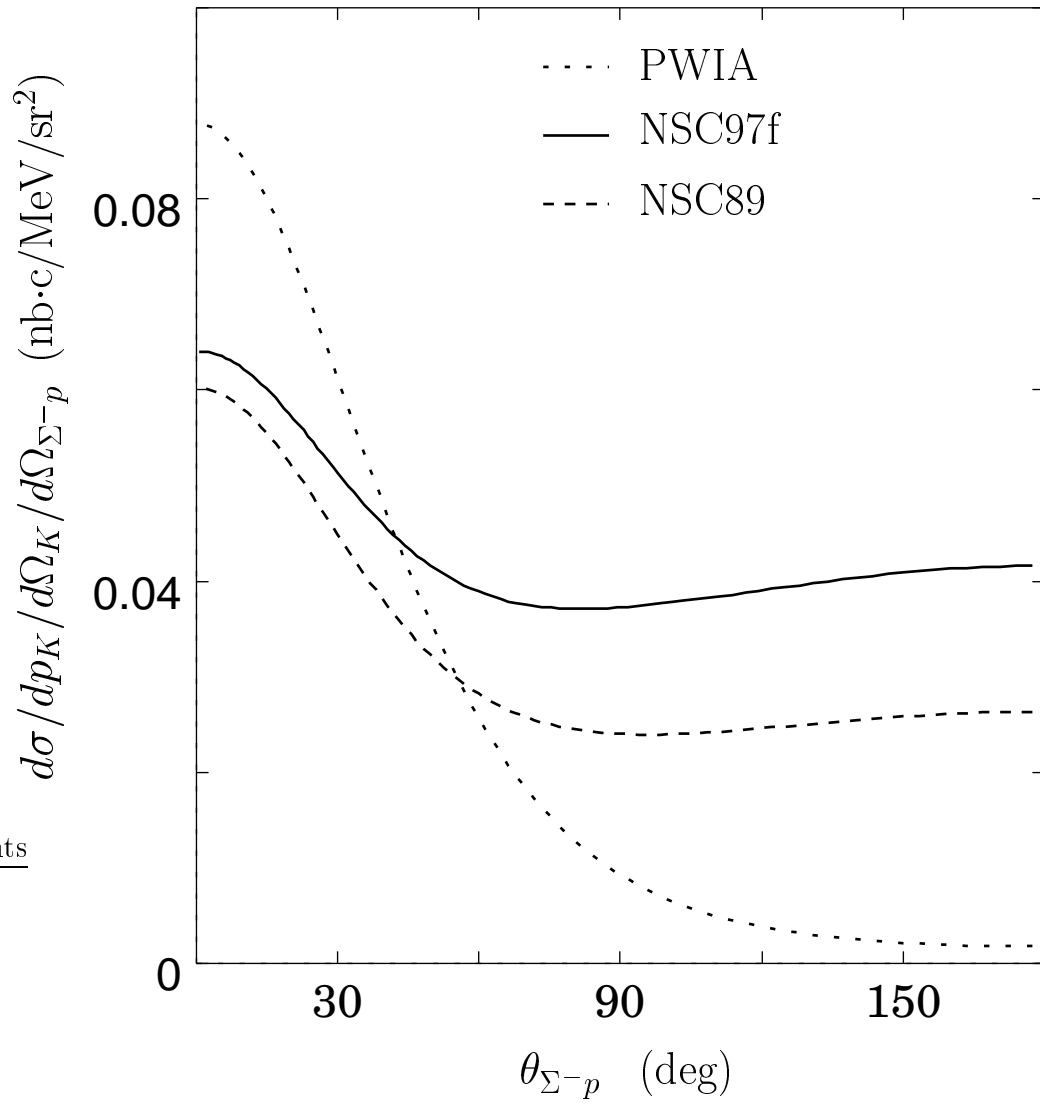


Fig. 10

